OPEN ACCESS
JOURNAL OF ADVANCED DIELECTRICS
Vol. 13, No. 6 (2023) 2345003 (7 pages)

DOI: 10.1142/S2010135X23450030

Bubble domain evolution in well-ordered $BiFeO_3$ nanocapacitors*

Fengyuan Zhang[†,‡,**], Guo Tian[§,¶], Lina Zhao[‖], Xingsen Gao[§,¶] and Jiangyu Li[†,‡]

[†]*Department of Materials Science and Engineering*
Southern University of Science and Technology, Shenzhen 518055, P. R. China

[‡]*Guangdong Provincial Key Laboratory of Functional Oxide Materials and Devices*
Southern University of Science and Technology, Shenzhen 518055, P. R. China

[§]*Institute for Advanced Materials, South China Academy of Advanced Optoelectronics*
South China Normal University, Guangzhou 510006, P. R. China

[¶]*Guangdong Provincial Key Laboratory of Optical Information Materials and Technology*
South China Normal University, Guangzhou 510006, P. R. China

[‖]*Institute of Data and Information, Tsinghua Shenzhen International Graduate School*
Shenzhen 518055, P. R. China

[‖]zhangfy@mail.sustech.edu.cn

Received 19 June 2023; Revised 12 July 2023; Accepted 23 July 2023; Published 11 August 2023

Ferroelectric nanocapacitors have attracted intensive research interest due to their novel functionalities and potential application in nanodevices. However, due to the lack of knowledge of domain evolution in isolated nanocapacitors, precise manipulation of topological domain switching in the nanocapacitor is still a challenge. Here, we report unique bubble and cylindrical domains in the well-ordered $BiFeO_3$ nanocapacitor array. The transformation of bubble, cylindrical and mono domains in isolated ferroelectric nanocapacitor has been demonstrated via scanning probe microscopy (SPM). The bubble domain can be erased to mono domain or written to cylindrical domain and mono domain by positive and negative voltage, respectively. Additionally, the domain evolution rules, which are mainly affected by the depolarization field, have been observed in the nanocapacitors with different domain structures. This work will be helpful in understanding the domain evolution in ferroelectric nanocapacitors and providing guidance on the manipulation of nanoscale topological domains.

Keywords: Ferroelectrics; SPM; domain evolution; bubble domain; nanocapacitor array.

1. Introduction

Ferroelectric materials with switchable spontaneous polarization have widely been investigated for memristors,[1,2] field-effect transistors[3] and nonvolatile random-access memories.[4–6] With the increasing demands for high-density data storage and device miniaturization, nanoscale ferroelectric capacitor arrays which promise individual addressability and high-density (~TB/inch) have attracted broader interest.[7–10] Especially in recent years, exotic topological domain configurations, such as bubble,[11–13] flux-closure,[14,15] center-type quad-domain,[16,17] vortex[18,19] and skyrmion,[20] which present novel features, have been found in ferroelectric nanostructures. For instance, stable topological domains can be deterministically switched while the corresponding domain wall conductivity is manipulated in isolated $BiFeO_3$ (BFO) nanoislands with hundreds of nanometers in lateral size.[17,21,22] The electrical erasure and writing of data by switching the topological domain further demonstrate its application potential in nanoelectronics devices.[23–26] As such, ferroelectric devices are based on the domain switching in nanoscale, it's essential to understand the domain switching evolution process of topological domains in nanocapacitors.

The domain evolution has been systematically studied on ferroelectric bulks, films, and capacitor structures theoretically and experimentally.[27–30] It has been shown that dimension has a significant influence on domain evolution process. In the micro-nanocapacitor, ferroelectric switching is coincident with bulks and films, including the steps of nucleation, growth and finally coalescence of domains as described in the classic Kolmogorov–Avrami–Ishibashi (KAI) model.[28,31] The nucleation location and domain growth way can be dramatically changed when the top electrode size reduced to 70 nm.[32] Besides, domain wall pining has also been observed in the same structure, suggesting that local defect has a significant effect on the switching process when the top electrode dimension is reduced.[33] Due to depolarization, strain

*This paper was originally submitted to the Special Issue on Ferroelectric Nanoelectronic Devices for Next-Generation Information Technology organized by Zheng Wen, Shuoguo Yuan, Zhen Fan and Yunya Liu.

**Corresponding author.

and local defects, the isolated ferroelectric nanocapacitors have more varieties of topological domains.[34,35] These factors that affected the initial domain structures in the isolated nanostructures may also play a significant role in the domain evolution. However, the domain evolution and reversibility of topological domain in isolated ferroelectric nanocapacitors are not yet clear.

Therefore, in this work, well-ordered isolated $SrRuO_3$/$BiFeO_3$ (SRO/BFO) nanodots were fabricated on conductive Nb-doped $SrTiO_3$ (NSTO). We present unique bubble domains and cylindrical domains in the SRO/BFO/NSTO nanocapacitor array and demonstrate the controlled transformation between these two domain states via scanning probe microscope (SPM). The domain evolution in the nanocapacitors with different domain structures was also investigated.

2. Experiment Details

Highly oriented conductive SRO and ferroelectric BFO-layered nanoislands array were fabricated on NSTO (100)-oriented single-crystal substrates by pulsed laser deposition (PLD) via thin anodic aluminum oxide (AAO) nanotemplate, as shown in Fig. S1. Both SRO and BFO were deposited at a growth temperature of 590°C in an oxygen atmosphere of 11 mTorr. The deposited SRO layer in the nanodot is considered as the top nanoelectrode, and the NSTO substrate is the bottom electrode. The well-ordered SRO/BFO nanoislands array, with AAO template removed by mechanical lift-off, is shown in Figs. 1(a) and 1(b). The BFO nanocapacitors have average height of ~8 nm and average lateral size of ~80 nm, which is identical to the lateral size of the pores in AAO template.

wThe epitaxial structure of these nanodots was verified by X-ray diffraction (XRD), as shown in Fig. S2. Rhombohedral phase BFO was observed from the XRD diffraction pattern of the SRO/BFO/NSTO nanocapacitor array. The surface topography and domain structure were revealed using a commercial SPM (Cypher, Asylum Research). Pt-coated conducting tips (EFM, Nanoworld) were operated at a resonance frequency of ~320 kHz and an AC bias amplitude of 0.4 V for vertical piezoelectric force microscopy (VPFM) in dual AC resonance tracking (DART) mode. Different DC biases were applied to the bottom electrode to switch the domain structures.

3. Results and Discussion

High-resolution SPM was used to excite and detect the topological domains in nanocapacitor array. The out-of-plane (OP) domain structures of the SRO/BFO/NSTO nanocapacitor array were examined by VPFM measurements (Fig. 1). As shown in Figs. 1(c) and 1(d), the polarization orientations in most nanocapacitors are downward, which are shown as dark colors in the phase image. Moreover, various domains can be found on these nanocapacitors. Figures 1(e) and 1(f) further illustrate the three-dimensional (3D) topological image superimposed by amplitude images (left) and phase images (right) of two typical domain structures in these nanocapacitors. The nanocapacitor with a cylindrical domain in Fig. 1(e) has an opposite phase, shown as white color in the phase image, while a clear ring-shaped domain wall feature can be found in the corresponding location in the amplitude image. Notably, the nanocapacitor with a bubble domain in Fig. 1(f) displays a single-phase image, while the amplitude shows a weak signal in the center of the capacitor. The nonuniform amplitude signal indicates the upward domain is already nucleated in the core of the capacitor, while the uniform phase signal indicates the downward polarization still dominates underneath

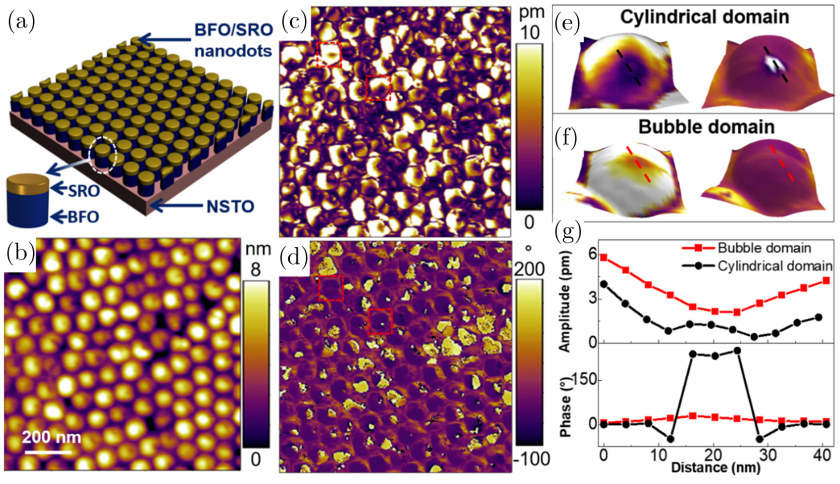

Fig. 1. Various domain structures in the SRO/BFO/NSTO nanocapacitor arrays. Schematic (a), topography (b), PFM amplitude (c) and phase (d) images of the SRO/BFO/NSTO nanocapacitor arrays. The isolated SRO/BFO nanodot (left bottom) is zoomed from the white dash circle in (a). The PFM amplitude (left) and phase (right) images of cylindrical domain (e) and bubble domain (f) in 100 × 100 nm^2 are superimposed with their 3D topographic images. The amplitude and phase cross-section profile (g) of cylindrical domain and bubble domain at the dash line in (e) and (f). The scale bar in (b) refers to (c) and (d).

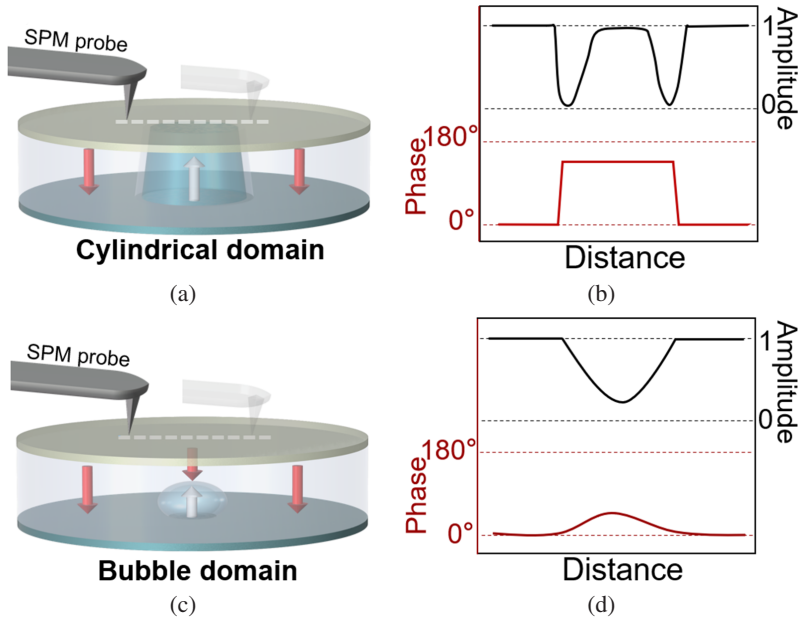

Fig. 2. (Color online) A sketch illustrating the VPFM signals from the cylindrical and bubble domains. (a) Cylindrical domain and (c) bubble domain configuration and their corresponding VPFM responses (b) and (d) at the cross-section lines. The white and red arrows represent the two different polarization directions (upward and downward) in each region.

the tip. The line profiles of the amplitude and phase images of these domain structures show different shapes (Fig. 1(g)). The amplitude and phase features of these domain structure match with previously reported cylindrical domain and bubble domain.[11,36] Besides, the size of the bubble domain (~10 nm) and cylindrical domain (~15 nm) in the nanocapacitors is also similar with the reported size.

The normal cylindrical domain can be clearly captured by the SPM tip (Fig. 2(a)), presenting as a "W" shape in the amplitude cross-section profile, as shown in Figs. 1(g) and 2(b). The two depressions along the line scan correspond to the location of the 180° domain wall. Similar cylindrical domains in well-ordered PZT and BFO nanocapacitors were reported, respectively, by Gao *et al.*[12] and Hong *et al.*[37] However, the bubble domain presents very different behaviors in the VPFM as reported in the ultrathin PZT film with a suitable residual depolarization field.[36] As shown in the schematic diagram in Figs. 2(c) and 2(d), the ultrasmall size in both vertical and lateral direction results in a uniform or non-180° phase response when the SPM tip crosses the bubble domain. Moreover, the reversed polarization of bubble domain in the OP direction neutralizes part of the downward polarization, resulting in a reduced amplitude response. Therefore, the bubble domain presents as a "U" shape in the amplitude cross-section profile.

The formation mechanism of such unique domain structures in the SRO/BFO/NSTO nanocapacitor should be related to its sandwich structure. First, the initial downward polarization is due to the built-in fields from the work-function difference between the top/bottom electrodes and BFO. From the band structure analysis, we have found that the SRO, BFO and NSTO have work-functions of around 5.2, 4.7 and 4.08 eV, respectively, which produces built-in voltages in both interfaces.[8] The built-in voltage in the interface of SRO/BFO is $V_{built} = (Ø_{SRO}–Ø_{BFO})/e$ = ~0.5 V, and in the interface of NSTO/BFO is $V_{built} = (Ø_{BFO}–Ø_{NSTO})/e$ = ~0.62 V with the same orientation. The overall theoretical V_{built} = 1.12 V leads to the formation of the observed downward polarization. In addition, the cylindrical domain and bubble domain may be due to the competition between depolarization, strain and other factors.[37,38] On the one hand, in our epitaxial BFO nanodots on NSTO substrate, a large depolarization field is expected. The downward polarization collects positive surface charge, which can't be screened effectively because of the limited conductivity of NSTO substrate.[39] This caused a large depolarization field generated in these capacitors. On the other hand, due to the irregularities in size, shape and strain, some regions maybe easier to switching under the depolarization field than others.[40,41] For instance, large strain energy exists near the center of the topological domain where dipoles turn their directions sharply.[34,41] Therefore, the opposite polarizations are very likely to appear in the center of the nanostructure, as shown in Figs. 1(e) and 1(f).

To study the reversibility between cylindrical domain and bubble domain, we applied electric voltage from the bottom electrode and recorded the domain transformation in two nanocapacitors with different initial domains by SPM tip. Figure 3(a) shows the 100 nm × 100 nm VPFM phase and amplitude images of the as grown nanocapacitor with cylindrical domain. 180° phase flipping and a clear domain wall were observed in the initial state. Electrical erasure of the cylindrical domain was carried out with small negative

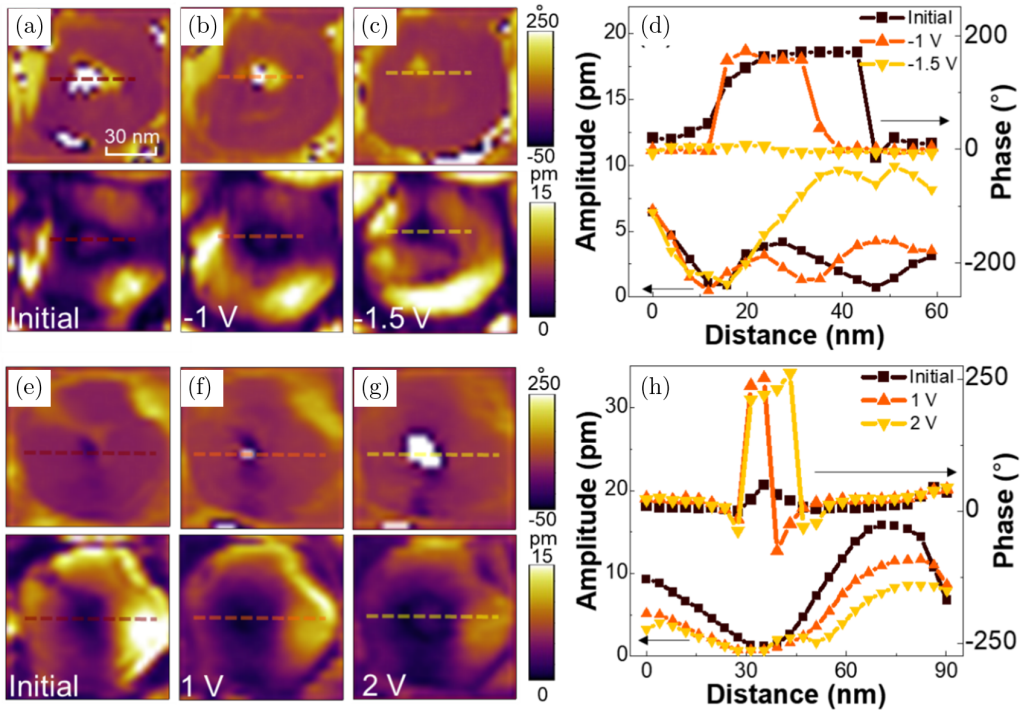

Fig. 3. PFM phase (top) and amplitude (bottom) images of two pristine nanocapacitors with cylindrical domain (a) and bubble domain (e). PFM phase (top) and amplitude (bottom) images of each nanocapacitor after electrical switching with negative voltage (−1 V (b), −1.5 V (c)) and positive voltage (1 V (f), 2 V (g)), respectively. The amplitude and phase cross-section profiles at the dash lines in (a)–(c) and (e), (g) show the transformation of cylindrical domain to bubble domain (d) and bubble domain to cylindrical domain (h), respectively. The scale bar in (a) refers to (b), (c) and (e)–(g).

voltages (−1 V, −1.5 V) applied from the bottom electrode. The cylindrical domain in the nanocapacitor was reduced and successfully transforming into bubble domain with a dark spot in the amplitude image at −1.5 V (Figs. 3(b) and 3(c)). The corresponding line profile at each state clearly shows the domain wall shifting from the right to the left side until a typical "U" shape amplitude and non-180° phase were generated (Fig. 3(d)). In addition, a reversible process from bubble domains to cylindrical domains was demonstrated in a nanocapacitor with an initial states of bubble domain (Fig. 3(e)). Positive voltages (1 V, 2 V) were applied from the bottom electrode to promote the growth of bubble domains into cylindrical domains (Figs. 3(f) and 3(g)). The 180° phase flipping was observed in the phase image at 1 V, but the domain wall was unclear due to the ultrasmall domain size (~5 nm) which is below the resolution of SPM tip. The "W" shape domain wall obtained at 2 V indicates a standard cylindrical domain was successfully transformed from bubble domain (Fig. 3(h)).

To gain further insight into the influence of the voltages on the domain growth in the unique bubble domain, we applied both negative and positive voltage via the bottom electrode to investigate the evolution of bubble domain to mono domain. Figure 4 shows a series of VPFM phase, amplitudes images and schematic diagrams that display the bubble domain evolution process. The amplitude and phase images in Figs. 4(a)–4(d) correspond to each domain state in the schematic diagram in Fig. 4(e). The pristine bubble domains are shown in the ii state in Figs. 4(a), 4(b) and iii state in Figs. 4(c) and 4(d). A series of applied voltages from 0.5 V to 8 V were applied to the nanocapacitor (Figs. 4(a), 4(b) and S3a), while voltages from −0.5 V to −1.5 V were applied to another nanocapacitor (Figs. 4(c) and 4(d)). Interestingly, even though the phase images didn't change below 2 V, the amplitude images shown the dark region (low amplitude) was expanding, and the central amplitude signal was weaker as the applied biases increased. These results indicate the bubble domain expands both in vertical and lateral direction at this stage, but nucleation growth along the thickness direction has not yet reached the other electrode to form the cylindrical domain. Considering the large diameter-height ratio of the nanodots, the domain wall seems moves faster in the in-plane direction than the OP direction during this process. In addition, after one nucleation occurs, the polarization switching mechanism relies solely on the motion of domain walls, as this process effectively decreases the nucleation energy. The bubble domain transformed into cylindrical domain (iv state) at 2 V and transformed into upward mono domain (vii state) at 7 V. The bubble domain can also be reversed switching to downward mono domain with negative voltage applied to the bottom electrode (Figs. 4(c) and 4(d)). Figure 4(d) shows the low amplitude region in the center of the nanocapacitor is

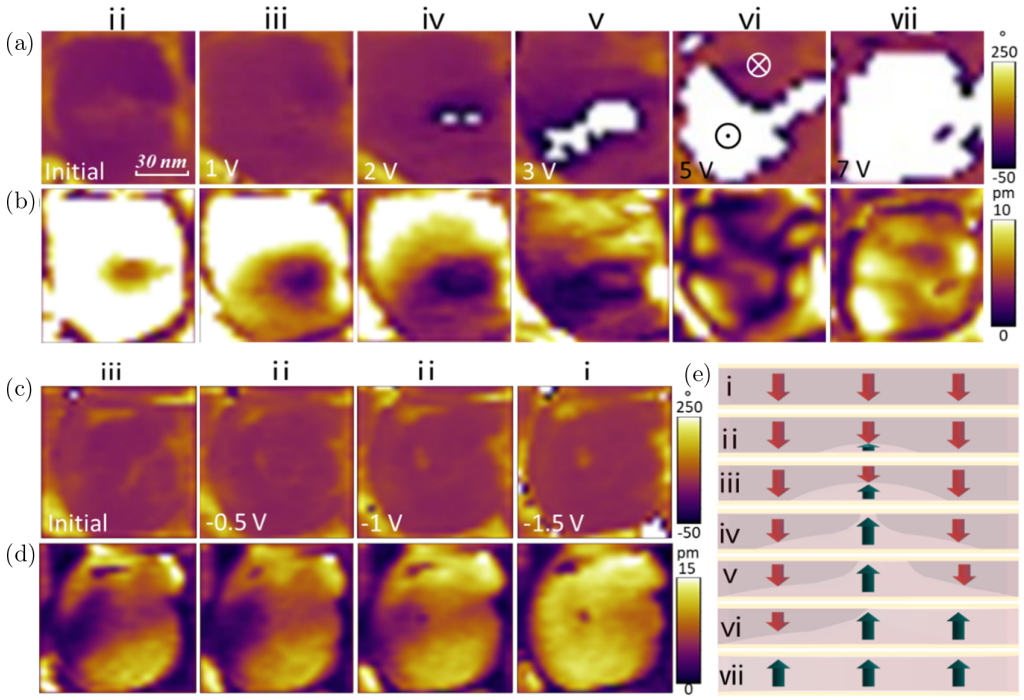

Fig. 4. Bubble domain evolution. Phase (a), (c) and amplitude (b), (d) of the evolution process of bubble domains to mono domain with upward polarization (a), (b) and downward polarization (c) and (d) by electrical writing with positive voltage and negative voltage (applied to the bottom electrode), respectively. Schematic description of vertical domain configurations at different stages inside a nanocapacitor. ii and iii indicates bubble domains, while i and vii indicate mono domains with downward polarization and upward polarization, respectively. The red and green arrows indicate downward and upward polarization, respectively. The scale bar in (a) refers to (b)–(d).

vanishing with the increased negative voltage, corresponding to the iii to i states in the schematic diagram in Fig. 4(e).

The domain evolution in other nanocapacitors with different initial domain structures (cylindrical domain and double domain) is also demonstrated in Fig. S3(b, c). The polarization orientations in these nanocapacitors all changed dramatically when increased positive voltages were applied to the bottom electrode. However, due to the different initial states, they have different evolution process. In order to show the difference of domain evolution more clearly, we quantitatively analyzed the switched region that varies with applied voltage in each selected nanocapacitor in Fig. 5. The domains in the nanocapacitors are not standard circle shapes in the evolution process, so the percentage of upward polarization region to the total nanocapacitor area was used in the plot. In the capacitors with bubble domain and cylindrical domain, the domain (switched area) growth quadratically with the applied voltage after iv state (Figs. 5(a) and 5(b)). After the domain area reaches a certain value, around half of the nanocapacitor (vi state), the domain growth becomes linear with the applied

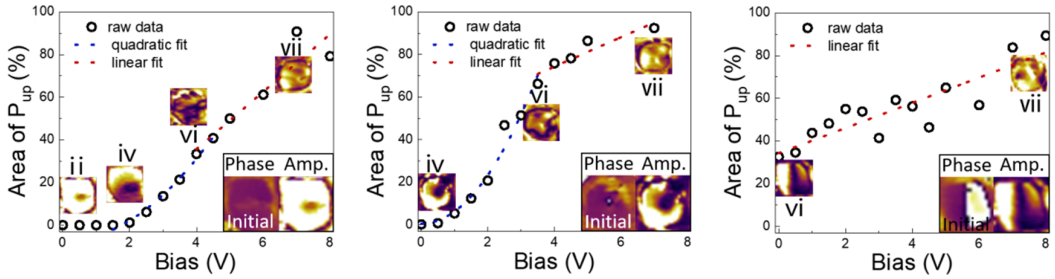

Fig. 5. (Color online) Dependence of the upward domain area on writing voltage. The plots of upward polarization area verse applied bias on the nanocapacitors with different initial domain structures, which are bubble domain (a), cylindrical domain (b) and double domain (c), respectively. The phase and amplitude images of the initial domain are inserted in the bottom right of each plot. The amplitude images at certain applied voltages are inserted in the plots, the Roman numeral corresponding to the domain state in Fig. 4(e). The circles represent the experimental data, while the blue and red dash lines represent quadratic and linear fitted data.

voltage until fully switched (vii state) in the whole capacitor (Figs. 5(a) and 5(c)). Unlike the switched area which is quadratic to voltage in the SPM tip/thin film system, the relationship between switched area and voltage is more complicated in the nanocapacitors.[27,42]

As we know, the formation and growth of domains in these nanocapacitors are affected by depolarization, domain wall energy and elastic energy. The depolarization field is in the same direction of the applied electric field and plays a major role in the nanocapacitor when downward polarization dominates the polarization orientation. The large depolarization field also enables the switched domain to relax to its initial state after tens of minutes in these nanocapacitors. Domains tend to lateral growth at the early stage to reduce the depolarization field, as shown in ii and iii state in Fig. 4(e). Later, domains permeated the entire thickness (iv state) can be formed due to the large domain wall energy and elastic energy. Domains with sharp domain walls rapidly grow with the applied voltage until depolarization changes into the opposite direction when upward polarization dominates the polarization orientation (vi state) in a nanocapacitor. Besides, both the double domain and other domains grow slower after the vi state, maybe due to the depolarization opposite to the applied electric field or domain wall pining.

In summary, we have investigated different domain structures and the electric conditions for their domain transformation, such as bubble domain and cylindrical domain, on well-ordered SRO/BFO/NSTO nanocapacitors and succeeded in capturing the voltage-dependent domain evolution in nanocapacitors with different domain structures. The possible formation mechanisms of the various domain structures in the nanocapacitor array were discussed. The upward polarization region is easy to appear in the center of the domain where high strain energy may exist, due to the large depolarization field in the nanocapacitors. Moreover, due to the finite size and unique domain structures, the voltage-dependent domain evolution in such isolated nanocapacitors does not follow the models previously proposed on film, large capacitors, or film-based nanocapacitors, i.e., the nucleation position is likely to occur at the center of the nanocapacitor. The domain tends to laterally grow at the very beginning in bubble domain. The domain area growth is linear from quadratically when the domain half-switches in the nanocapacitor. The results help better understand the evolution in different domains, especially bubble domain in ferroelectric nanocapacitor which is promising for potential applications in high-density nonvolatile memory devices.

Acknowledgments

This research was supported by Guangdong Basic and Applied Basic Research Foundation (No. 2021A1515110155), National Key Research and Development Program of China (No. 2022YFF0706100), the National Natural Science Foundation of China (Nos. 92066203, 12192213, U22A20117, 52002134), the Guangdong Provincial Key Laboratory Program from Guangdong Science and Technology Department (No. 2021B1212040001), the Science and Technology Projects in Guangzhou (No. 202201000008), The authors also acknowledge the assistance of Core Research Facilities and Center for Computational Science and Engineering at Southern University of Science and Technology, and Li acknowledges the financial support for Outstanding Talents Training Fund in Shenzhen.

References

[1]A. Chanthbouala *et al.*, A ferroelectric memristor, *Nat. Mater.* **11**(10), 860 (2012), doi:10.1038/nmat3415.

[2]Z. Chen *et al.*, All-ferroelectric implementation of reservoir computing, *Nat. Commun.* **14**(1), 3585 (2023), doi:10.1038/s41467-023-39371-y.

[3]A. I. Khan, A. Keshavarzi and S. Datta, The future of ferroelectric field-effect transistor technology, *Nat. Electron.* **3**(10), 588 (2020), doi:10.1038/s41928-020-00492-7.

[4]T. Mikolajick, U. Schroeder and S. Slesazeck, The past, the present, and the future of ferroelectric memories, *IEEE Trans. Electron Devices* **67**(4), 1434 (2020), doi:10.1109/ted.2020.2976148.

[5]F. Zhang *et al.*, Boosting polarization switching-induced current injection by mechanical force in ferroelectric thin films, *ACS Appl. Mater. Interfaces* **13**(22), 26180 (2021), doi:10.1021/acsami.1c04912.

[6]B. Y. Cui *et al.*, Ferroelectric photosensor network: An advanced hardware solution to real-time machine vision, *Nat. Commun.* **13**(1), 1707 (2022), doi:10.1038/s41467-022-29364-8.

[7]F. Y. Zhang *et al.*, Unique nano-domain structures in self-assembled $BiFeO_3$ and $Pb(Zr,Ti)O_3$ ferroelectric nanocapacitors, *Nanotechnology* **27**(1), 9 (2016), doi:10.1088/0957-4484/27/1/015703.

[8]L. N. Zhao *et al.*, Current rectifying and resistive switching in high density $BiFeO_3$ nanocapacitor arrays on Nb-$SrTiO_3$ substrates, *Sci. Rep.* **5**, 9680 (2015), doi:10.1038/srep09680.

[9]H. Fan *et al.*, Large electroresistance and tunable photovoltaic properties of ferroelectric nanoscale capacitors based on ultrathin super-tetragonal $BiFeO_3$ films, *J. Mater. Chem. C* **5**(13), 3323 (2017), doi:10.1039/c6tc04615k.

[10]F. Y. Zhang, D. Edwards, X. Deng, Y. D. Wang, J. I. Kilpatrick, N. Bassiri-Gharb, A. Kumar, D. Y. Chen, X. S. Gao and B. J. Rodriguez, Investigation of AFM-based machining of ferroelectric thin films at the nanoscale, *J. Appl. Phys.* **127**(3), 034103 (2020), doi:10.1063/1.5133018.

[11]Q. Zhang, L. Xie, G. Liu, S. Prokhorenko, Y. Nahas, X. Pan, L. Bellaiche, A. Gruverman and N. Valanoor, Nanoscale bubble domains and topological transitions in ultrathin ferroelectric films, *Adv. Mater.* **29**(46), 1702375 (2017), doi:10.1002/adma.201702375.

[12]X. S. Gao, F. Xue, M. H. Qin, J. M. Liu, B. J. Rodriguez, L. F. Liu, M. Alexe and D. Hesse, Bubble polarization domain patterns in periodically ordered epitaxial ferroelectric nanodot arrays, *J. Appl. Phys.* **110**(5), 052006 (2011), doi:10.1063/1.3623766.

[13]X. Zhang *et al.*, Creation and erasure of polar bubble domains in $PbTiO_3$ films by mechanical stress and light illuminations, *J. Materiomics* **9**, 626 (2023), doi:10.1016/j.jmat.2023.01.004.

[14]Y. L. Tang *et al.*, Observation of a periodic array of flux-closure quadrants in strained ferroelectric $PbTiO_3$ films, *Science* **348**(6234), 547 (2015), doi:10.1126/science.1259869.

[15]J. J. P. Peters, G. Apachitei, R. Beanland, M. Alexe and A. M. Sanchez, Polarization curling and flux closures in multiferroic tunnel junctions, *Nat. Commun.* **7**, 13484 (2016), doi:10.1038/ncomms13484.

[16]Z. W. Li *et al.*, High-density array of ferroelectric nanodots with robust and reversibly switchable topological domain states, *Sci. Adv.* **3**(8), e1700919 (2017), doi:10.1126/sciadv.1700919.
[17]J. Ma *et al.*, Controllable conductive readout in self-assembled, topologically confined ferroelectric domain walls, *Nat. Nanotechnol.* **13**(10), 947 (2018), doi:10.1038/s41565-018-0204-1.
[18]Z. Hong *et al.*, Stability of polar vortex lattice in ferroelectric superlattices, *Nano Lett.* **17**(4), 2246 (2017), doi:10.1021/acs.nanolett.6b04875.
[19]N. Balke *et al.*, Enhanced electric conductivity at ferroelectric vortex cores in $BiFeO_3$, *Nat. Phys.* **8**(1), 81 (2012), doi:10.1038/nphys2132.
[20]S. Das *et al.*, Observation of room-temperature polar skyrmions, *Nature* **568**(7752), 368 (2019), doi:10.1038/s41586-019-1092-8.
[21]G. Tian *et al.*, Manipulation of conductive domain walls in confined ferroelectric nanoislands, *Adv. Funct. Mater.* **29**(32), 1807276 (2019), doi:10.1002/adfm.201807276.
[22]G. Tian *et al.*, Templated growth strategy for highly ordered topological ferroelectric quad-domain textures, *Appl. Phys. Rev.* **10**(2), 021413 (2023), doi:10.1063/5.0144979.
[23]J. Wang *et al.*, Ferroelectric domain-wall logic units, *Nat. Commun.* **13**(1), 3255 (2022), doi:10.1038/s41467-022-30983-4.
[24]W. Yang *et al*., Nonvolatile ferroelectric-domain-wall memory embedded in a complex topological domain structure, *Adv. Mater.* **34**(10), 2107711 (2022), doi:10.1002/adma.202107711.
[25]M. Chen, J. Ma, R.-C. Peng, Q. Zhang, J. Wang, Y. Liang, J. Wu, L.-Q. Chen, J. Ma and C.-W. Nan, Robust polarization switching in self-assembled $BiFeO_3$ nanoislands with quad-domain structures, *Acta Mater.* **175**, 324 (2019), doi:10.1016/j.actamat.2019.06.016.
[26]D. Zheng *et al.*, Controlled manipulation of conductive ferroelectric domain walls and nanoscale domains in $BiFeO_3$ thin films, *J. Materiomics* **8**(2), 274 (2022), doi:10.1016/j.jmat.2021.10.003.
[27]M. Molotskii, Generation of ferroelectric domains in films using atomic force microscope, *J. Appl. Phys.* **97**(1), 014109 (2005), doi:10.1063/1.1823028.
[28]A. Gruverman, B. J. Rodriguez, C. Dehoff, J. D. Waldrep, A. I. Kingon, R. J. Nemanich and J. S. Cross, Direct studies of domain switching dynamics in thin film ferroelectric capacitors, *Appl. Phys. Lett.* **87**(8), 082902 (2005), doi:10.1063/1.2010605.
[29]S. M. Yang and Y. Kim, Nanoscale probing of ferroelectric domain switching using piezoresponse force microscopy, *J. Korean Ceram. Soc.* **56**(4), 340 (2019), doi:10.4191/kcers.2019.56.4.05.
[30]C. T. Nelson *et al*., Domain dynamics during ferroelectric switching, *Science* **334**(6058), 968 (2011), doi:10.1126/science.1206980.
[31]A. K. Tagantsev, I. Stolichnov, N. Setter, J. S. Cross and M. Tsukada, Non-Kolmogorov–Avrami switching kinetics in ferroelectric thin films, *Phys. Rev. B* **66**(21), 214109 (2002), doi:10.1103/PhysRevB.66.214109.
[32]Y. Kim, H. Han, W. Lee, S. Baik, D. Hesse and M. Alexe, Non-Kolmogorov–Avrami–Ishibashi switching dynamics in nanoscale ferroelectric capacitors, *Nano Lett.* **10**(4), 1266 (2010), doi:10.1021/nl9038339.
[33]Y. Kim, H. Hee, V. Ionela, L. Woo, H. Dietrich and A. Marin, Origins of domain wall pinning in ferroelectric nanocapacitors, *Nano Converg.* **1**(24), 1 (2014), doi:10.1186/s40580-014-0024-4.
[34]B. J. Rodriguez, X. S. Gao, L. F. Liu, W. Lee, I. I. Naumov, A. M. Bratkovsky, D. Hesse and M. Alexe, Vortex polarization states in nanoscale ferroelectric arrays, *Nano Lett.* **9**(3), 1127 (2009), doi:10.1021/nl8036646.
[35]H. Chen *et al.*, Complex center-type topological domain in ferroelectric nanoislands of rhombohedral $Pb(Zr_{0.7},Ti_{0.3})O_3$, *J. Appl. Phys.* **128**(22), 224103 (2020), doi:10.1063/5.0029743.
[36]Q. Zhang, S. Prokhorenko, Y. Nahas, L. Xie, L. Bellaiche, A. Gruverman and N. Valanoor, Deterministic switching of ferroelectric bubble nanodomains, *Adv. Funct. Mater.* **29**(28), 1808573 (2019), doi:10.1002/adfm.201808573.
[37]S. Hong *et al.*, Large resistive switching in Ferroelectric $BiFeO_3$ nano-island based switchable diodes, *Adv. Mater.* **25**(16), 2339 (2013), doi:10.1002/adma.201204839.
[38]C. Lichtensteiger, S. Fernandez-Pena, C. Weymann, P. Zubko and J.-M. Triscone, Tuning of the depolarization field and nanodomain structure in ferroelectric thin films, *Nano Lett.* **14**(8), 4205 (2014), doi:10.1021/nl404734z.
[39]Z. Fan *et al.*, Resistive switching induced by charge trapping/detrapping: A unified mechanism for colossal electroresistance in certain Nb:$SrTiO_3$-based heterojunctions, *J. Mater. Chem. C* **5**(29), 7317 (2017), doi:10.1039/c7tc02197f.
[40]H. Han, Y. J. Park, S. Baik, W. Lee, M. Alexe, D. Hesse and U. Goesele, Domain structures and piezoelectric properties of $Pb(Zr_{(0.2)}Ti_{(0.8)})O_{(3)}$ nanocapacitors, *J. Appl. Phys.* **108**(4), 044102 (2010), doi:10.1063/1.3475476.
[41]M.-J. Han, Y.-J. Wang, Y.-L. Tang, Y.-L. Zhu, J.-Y. Ma, W.-R. Geng, M.-J. Zou, Y.-P. Feng, N.-B. Zhang and X.-L. Ma, Shape and surface charge modulation of topological domains in oxide multiferroics, *J. Phys. Chem. C* **123**(4), 2557 (2019), doi:10.1021/acs.jpcc.8b10678.
[42]J. Pan, T. Men, X. Xu, Z. Xu, Q. Li, X.-C. Chu, Y. Shen, B. Han and K. Wang, Domain growth dynamics in PMN-PT ferroelectric thin films, *J. Mater. Sci.* **54**(15), 10600 (2019), doi:10.1007/s10853-019-03563-z.